

# Novel Electronic Properties of the Hubbard Model on a Frustrated Triangular Lattice

Bumsoo Kyung

Département de physique and Regroupement québécois sur les matériaux de pointe,  
Université de Sherbrooke, Sherbrooke, Québec, J1K 2R1, Canada

(Dated: January 25, 2020)

We study novel electronic properties of the Hubbard model on a triangular lattice using the cellular dynamical mean-field theory. The interplay of strong geometric frustration and electron correlations causes a Mott transition at the Hubbard interaction  $U/t = 10.5$  and an unusual suppression of low energy spin excitations. Doping of a triangular Mott insulator leads to a quasiparticle peak (no pseudogap) at the Fermi surface and to an unexpected increase of low energy spin excitations, in stark contrast to the unfrustrated square lattice case. The present results give much insight into strongly frustrated electronic systems. A few predictions are made.

PACS numbers: 71.10.Fd, 71.27.+a, 71.30.+h, 71.10.-w

Geometric frustration with strong electronic correlations is one of the main issues in modern condensed matter physics. The simplest example is the two dimensional Heisenberg model (large  $U$  limit of the half-filled Hubbard model) on a triangular lattice in which all three spins cannot be antiparallel at the same time. The frustrated triangular lattice geometry was argued by Anderson [1] to provide an ideal background for the long sought resonating valence bond (RVB) state. The interplay of strong geometric frustration and electronic correlations is expected to lead to some exotic phases. Recent discovery of superconductivity in the triangular lattice compound  $\text{Na}_x\text{CoO}_2 \cdot y\text{H}_2\text{O}$  [2] and a possible quantum spin liquid state in the anisotropic triangular lattice organic material  $\kappa$ -(ET)<sub>2</sub>Cu<sub>2</sub>(CN)<sub>3</sub> [3] has further stimulated interest in strongly frustrated electronic systems.

The electronic properties of the Hubbard and  $t - J$  models on a triangular lattice have been studied using various analytical and numerical techniques. These include a high-temperature expansion [4], a slave-boson mean-field [5, 6, 7], an RG method [8], an exact diagonalization (ED) technique [9, 10, 11], a quantum Monte Carlo (QMC) simulation [12], a dynamical mean-field theory (DMFT) [13, 14], and a variational Monte Carlo approach [15]. However, some of the central issues on a triangular lattice have not been clearly addressed and still remain an open question: what is the nature of the ground state of a doped triangular Mott insulator? is it an RVB-like state (manifested as the presence of a pseudogap at small doping like on an unfrustrated square lattice) or a correlated Fermi liquid? what are qualitative differences between the triangular and square lattice systems? In this paper, utilizing recent theoretical progress in quantum cluster methods, we address these issues and provide much insight into novel electronic properties in strongly frustrated electronic systems.

The two-dimensional Hubbard model on a triangular lattice is described by

$$H = \sum_{\langle ij \rangle, \sigma} t_{ij} c_{i\sigma}^\dagger c_{j\sigma} + U \sum_i n_{i\uparrow} n_{i\downarrow} - \mu \sum_{i\sigma} c_{i\sigma}^\dagger c_{i\sigma}, \quad (1)$$

where  $c_{i\sigma}^\dagger$  ( $c_{i\sigma}$ ) are creation (annihilation) operators for

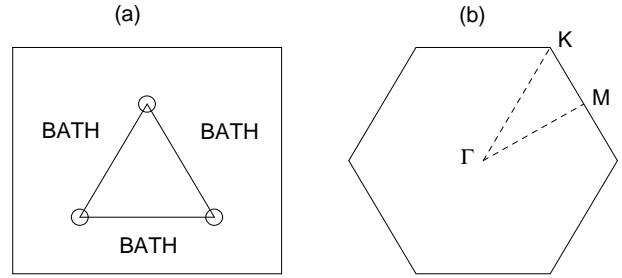


FIG. 1: (a) Three-site quantum cluster embedded in an effective medium (called bath) and (b) first Brillouin zone of the triangular lattice.

electrons of spin  $\sigma$ ,  $n_{i\sigma} = c_{i\sigma}^\dagger c_{i\sigma}$  is the density of  $\sigma$  spin electrons,  $U$  is the on-site repulsive interaction, and  $\mu$  is the chemical potential controlling the electron density.

To describe strong electron correlations and geometric frustration accurately, we use cellular dynamical mean-field theory (CDMFT) [16], a quantum cluster approach that allows one to extend DMFT [17] to incorporate short-range spatial correlations explicitly. CDMFT has been benchmarked and is accurate even in one dimension [18, 19]. The infinite lattice is tiled with identical clusters of size  $N_c$ , and the degrees of freedom in the cluster are treated exactly while the remaining ones are replaced by a bath of non-interacting electrons that is determined self-consistently (Fig. 1(a)). To solve the quantum cluster embedded in an effective medium, we consider a cluster-bath Hamiltonian of the form [16, 18, 20]

$$H = \sum_{\langle \mu\nu \rangle, \sigma} t_{\mu\nu} c_{\mu\sigma}^\dagger c_{\nu\sigma} + U \sum_{\mu} n_{\mu\uparrow} n_{\mu\downarrow} + \sum_{m, \sigma, \alpha} \varepsilon_{m\sigma}^\alpha a_{m\sigma}^\dagger a_{m\sigma}^\alpha + \sum_{m, \mu, \sigma, \alpha} V_{m\mu\sigma}^\alpha (a_{m\sigma}^\dagger c_{\mu\sigma} + \text{H.c.}). \quad (2)$$

Here the indices  $\mu, \nu = 1, \dots, N_c$  label sites within the cluster, and  $c_{\mu\sigma}$  and  $a_{m\sigma}^\alpha$  annihilate electrons on the cluster and the bath, respectively.  $t_{\mu\nu}$  are the hopping matrix elements within the cluster (the chemical potential  $\mu$  is absorbed here),  $\varepsilon_{m\sigma}^\alpha$  are the bath energies and  $V_{m\mu\sigma}^\alpha$  are

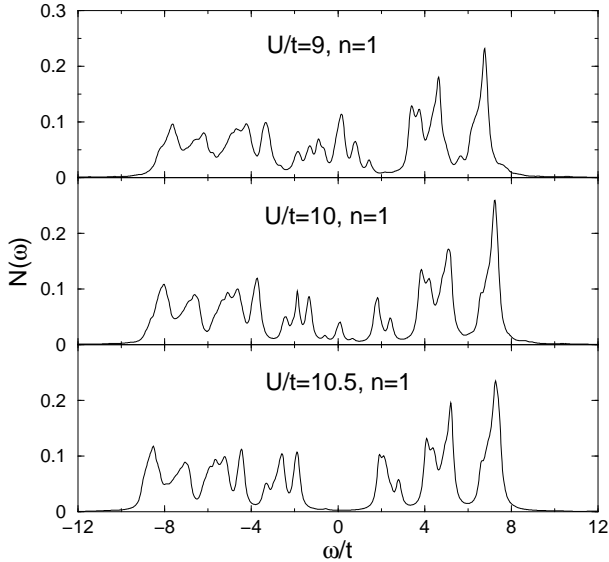


FIG. 2: Density of states  $N(\omega)$  on a triangular lattice at half-filling ( $n = 1$ ) with increasing  $U/t$ .

the bath-cluster hybridization matrices. The exact diagonalization method [21] is used to solve the cluster-bath Hamiltonian Eq. 2 at zero temperature, which has the advantage of computing dynamical quantities directly in real frequency and of treating the large  $U$  regime without difficulty. In the present study we used  $N_c = 3$  sites for the cluster and  $N_b = 9$  sites for the bath with  $m = 1, 2, 3$ ,  $\alpha = 1, 2, 3$ . Although the present study focuses on a small cluster with additional 9 bath sites, we expect our results to be robust with respect to an increase in the cluster size. This was verified by our recent low (but finite) temperature CDMFT+QMC calculations [19] where at intermediate to strong coupling a 4-site cluster accounts for more than 95% of the correlation effect of the infinite size cluster in the single-particle spectrum. Quantitatively similar results were found for different bath sizes ( $N_b = 6$ ). In this paper we focus on the normal state properties at and near half-filling.

We first study the Mott transition of the half-filled Hubbard model on a triangular lattice. Among several physical quantities one can gauge to investigate the Mott transition, we present the density of states  $N(\omega)$  as a function of  $U/t$  shown in Fig. 2. For  $U/t < 10.5$  a small spectral weight remains near the Fermi energy reminiscent of the Kondo resonance observed in DMFT [17], although the details are different. When  $U/t$  approaches 10.5, the spectral weight of the central peak is completely pushed away from  $\omega = 0$  leading to an interaction-driven Mott insulator. This critical value of  $U/t$  is somewhat smaller than 12 obtained in the ED study of an isolated 12-site cluster [9] and in the DMFT analysis [14]. Beyond  $U/t = 10.5$  it becomes increasingly more difficult to find a convergent solution, since the ground state starts to become degenerate. The way how the Mott transition

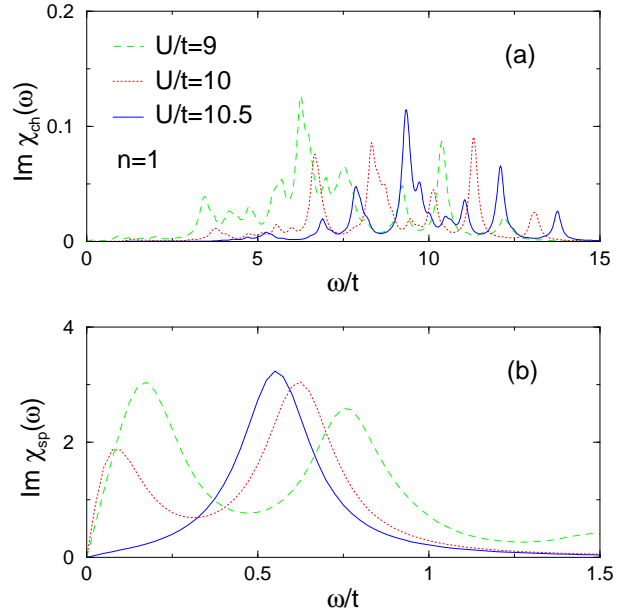


FIG. 3: (color online) Imaginary part of the local dynamical (a) charge and (b) spin correlation functions at half-filling with increasing  $U/t$ . The dashed, dotted and solid curves correspond to  $U/t=9, 10$  and  $10.5$ , respectively.

occurs on a frustrated triangular lattice is dramatically different from the unfrustrated square lattice case. In the latter [20], with increasing  $U/t$  the spectral weight always becomes a local minimum at the Fermi energy until it completely vanishes near  $U/t = 6$ .

Next we examine the local dynamical charge and spin correlation functions near the Mott transition shown in Fig. 3. With increasing  $U/t$  the low energy charge excitations are gradually depleted and transferred to high energy near  $\omega = U/t$ . On the other hand, the low energy spectrum in the spin correlation function undergoes a dramatic change near the Mott transition. As the Mott transition is approached, the primary low energy excitation near  $w/t = 0.2$  moves rapidly to the secondary peak near  $w/t = 0.5 - 0.6$  and eventually disappears. Namely, geometric frustration suppresses the low energy spin excitations, which is most strongly manifested in the insulating state ( $U/t = 10.5$ ). We found similar results for the nearest neighbor charge and spin correlation functions. This feature is in stark contrast to the square lattice case. In the latter, for the same range of  $U/t$  ( $9 - 10.5$ ) the low energy spin spectra are almost identical with a sharp primary peak near  $w/t = 0.25 - 0.3$  [22] and a secondary peak near  $w/t = 0.6 - 0.7$  similar to the case of  $U/t = 9$  on a triangular lattice. Near the range of  $U/t$  ( $4 - 6$ ) where a continuous crossover of a metal to an insulator occurs on a square lattice, with increasing  $U/t$  the low energy spin spectrum near  $w/t = 0.25$  becomes stronger, which is opposite to the behavior found on a triangular lattice.

Figure 4 shows the spectral function  $A(\vec{k}, \omega)$  for both

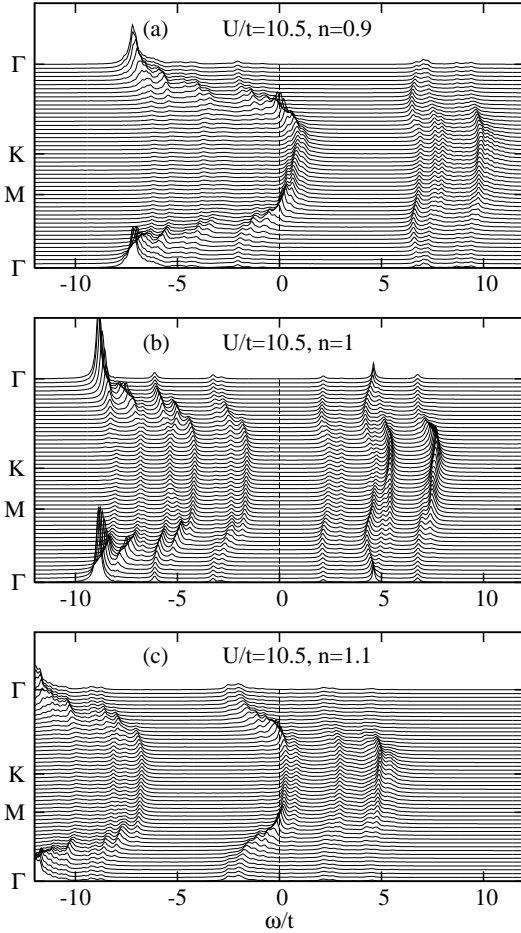


FIG. 4: Spectral function  $A(\vec{k}, \omega)$  for (a)  $n=0.9$ , (b)  $n=1$ , and (c)  $n=1.1$  along the path  $\Gamma$ -M-K- $\Gamma$  for  $U/t = 10.5$ .  $\Gamma$ , M, and K are defined in Fig. 1(b).

10% hole- and electron-dopings. Electron-doping corresponds to the negative sign of the hopping integral ( $t < 0$ ) in the  $t - J$  model. At half-filling (Fig. 4(b))  $A(\vec{k}, \omega)$  shows several features, which are similar to those on a square lattice [20]. Although they are weaker than on a square lattice, the low energy inner bands are clearly seen near the Fermi energy, which are caused by short-range spin correlations [20]. Upon hole- or electron-doping the Fermi level jumps to the nearest low energy band just like on a square lattice. This indicates the importance of short-range correlations even on a highly frustrated triangular lattice. The most dramatic difference, however, is that near half-filling there is no evidence of a (strong coupling) pseudogap unlike on a square lattice. It is more evident from the fact that  $A(\vec{k}, \omega)$  becomes sharper as  $\vec{k}$  approaches the Fermi surface. This is true for other fillings (5 – 30% hole- and electron-doping). Thus the present result clearly shows that a doped triangular Mott insulator is not an RVB-like state unlike on a square lat-

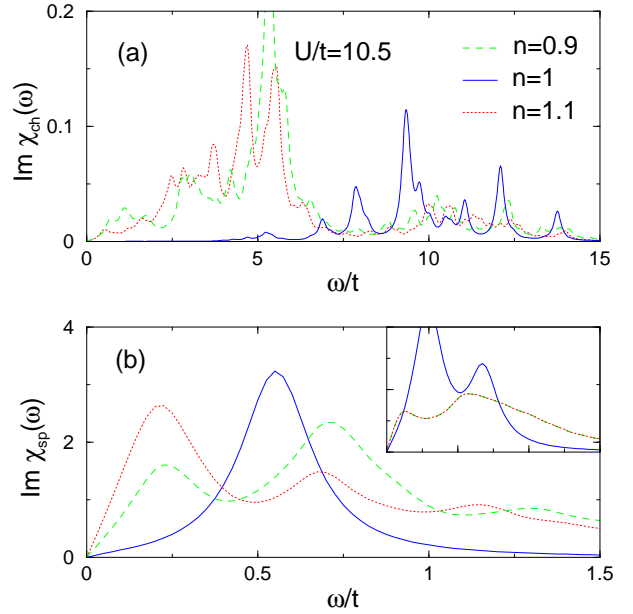


FIG. 5: (color online) Imaginary part of the local dynamical (a) charge and (b) spin correlation functions for  $U/t = 10.5$  with doping. The inset in (b) is the imaginary part of the local dynamical spin correlation function for the unfrustrated square lattice case. The dashed, solid, and dotted curves correspond to  $n=0.9$ , 1 and 1.1, respectively.

tice [20]. The absence of the pseudogap is ascribed to too much frustration of short-range spin correlations on a triangular lattice as shown in Fig. 6. Here we predict that near half-filling  $A(\vec{k}, \omega)$  has a quasiparticle peak at the Fermi surface, which should be tested by angle resolved photoemission spectroscopy (ARPES) experiments on a triangular lattice compound such as  $\text{Na}_x\text{CoO}_2$  at small doping.

Next let us examine the local dynamical charge and spin correlation functions upon doping shown in Fig. 5. As expected, with doping the high energy charge excitations at half-filling move to the low energy due to the metallic nature of electrons. The most surprising result comes from the spin correlation function. The primary low energy peak near  $w/t = 0.2$ , which has vanished in the insulating state due to strong geometric frustration shown in Fig. 3, *reappears* upon doping. This is completely opposite to the square lattice case (the inset in Fig. 5(b)) where the primary low energy peak weakens rapidly with doping. On a triangular lattice geometric frustration is released by doping. Here we also predict that inelastic neutron scattering experiments should observe the increase of low energy spin excitations with doping of a triangular Mott insulator such as  $\text{Na}_x\text{CoO}_2$ .

Finally we study the static local and nearest neighbor spin correlations with doping for both triangular and square lattices shown in Fig. 6. For the local quantity  $\langle S_1^z \cdot S_1^z \rangle$  they are similar in both cases, although the particle-hole symmetry is broken on a triangular lattice.

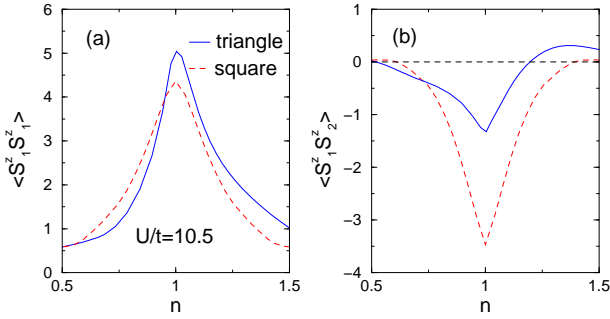


FIG. 6: (color online) Static (a) local and (b) nearest neighbor spin correlations for  $U/t = 10.5$  with doping. The dashed curves are the corresponding results on a square lattice.

The most dramatic difference is seen in the nearest neighbor spin correlation  $\langle S_1^z \cdot S_2^z \rangle$ . First of all the nearest neighbor spin correlation is much reduced compared with a square lattice because of strong geometric frustration. While it remains essentially antiferromagnetic (negative sign) on a square lattice, it becomes rapidly *ferromagnetic* on the electron-doped side of the triangular lattice. The strong asymmetric behavior on a triangular lattice that the spin correlation becomes ferromagnetic only on the electron-doping side is in agreement with the high temperature expansion study of the  $t - J$  model by Koretsune *et al.* [4] and the analysis of an isolated three-site cluster by Merino *et al.* [13]. It is also noteworthy that the ferromagnetic correlation is maximum near  $n = 1.35$  ( $x = 0.35$ ), where superconductivity has been observed in  $\text{Na}_x\text{CoO}_2 \cdot y\text{H}_2\text{O}$  [2]. Although the small cluster used in this work ( $N_c = 3$ ) does not allow us to study which gap symmetry (p or f) is more stable and how robust this result would be with respect to several parameters such

as doping level [23], our present result offers a natural route to *spin triplet* superconductivity in this compound within the one-band Hubbard model (without assuming the existence of unobserved hole pockets near  $\vec{k} = K$ ).

Sodium cobaltate  $\text{Na}_x\text{CoO}_2$  has shown a rich phase diagram [24]. These include a superconducting phase near  $x = 0.3 - 0.35$  upon hydration, a charge-ordered insulating phase at  $x = 0.5$  and a spin-density-wave metallic phase above  $x = 0.75$ . Since the charge-ordered insulating phase in cobaltates is observed at  $x = 1/2$  doping which is not a natural commensurate value ( $x = 1/3$  or  $2/3$ ) of the triangular lattice, the one-band Hubbard model alone would not be enough to describe this phase. It requires longer-range Coulomb interaction  $V_{ij}$ , which we did not consider in this work.

In conclusion, we have studied novel electronic properties of the Hubbard model on a triangular lattice using the cellular dynamical mean-field theory. The interplay of strong geometric frustration and electron correlations is responsible for many unconventional features, which are in stark contrast to the unfrustrated square lattice case. In particular the absence of an RVB-like state upon doping is ascribed to too much frustration of short-range spin correlations on a triangular lattice. We predict that upon doping a triangular Mott insulator ARPES should observe a quasiparticle peak (no pseudogap) at the Fermi surface and that inelastic neutron scattering should find an increase of low energy spin excitations.

We thank P. W. Anderson, S. R. Hassan, and A. -M. S. Tremblay for useful discussions, and A. -M. S. Tremblay for critical reading of the manuscript. Computations were performed on the Elix2 Beowulf cluster and on the Dell cluster of the RQCHP. The present work was supported by NSERC (Canada), FQRNT (Québec), CFI (Canada), and CIAR.

- 
- [1] P. W. Anderson, Mat. Res. Bull. **8**, 153 (1973); Science **235**, 1196 (1987).  
[2] K. Takada *et al.*, Nature (London) **422**, 53 (2003).  
[3] Y. Shimizu *et al.*, Phys. Rev. Lett. **91**, 107001 (2003).  
[4] T. Koretsune and M. Ogata, Phys. Rev. Lett. **89**, 116401 (2002).  
[5] G. Baskaran, Phys. Rev. Lett. **91**, 097003 (2003).  
[6] B. Kumar and B. S. Shastry, Phys. Rev. B **68**, 104508 (2003).  
[7] Q.-H. Wang, D.-H. Lee, and P. A. Lee, Phys. Rev. B **69**, 092504 (2004).  
[8] C. Honerkamp, Phys. Rev. B **68**, 104510 (2003).  
[9] M. Capone, L. Capriotti, F. Becca, and S. Caprara, Phys. Rev. B **63**, 085104 (2001).  
[10] J. O. Haerter and B. S. Shastry, Phys. Rev. Lett. **95**, 087202 (2005); J. O. Haerter, M. R. Peterson, and B. S. Shastry, cond-mat/0608005.  
[11] T. Tohyama, cond-mat/0605007.  
[12] N. Bulut, W. Koshiba, and S. Maekawa, Phys. Rev. Lett. **95**, 037001 (2005).  
[13] J. Merino, B. J. Powell, and R. H. McKenzie, Phys. Rev. B **73**, 235107 (2006).  
[14] K. Aryanpour, W. E. Pickett, and R. T. Scalettar, Phys. Rev. B **74**, 085117 (2006).  
[15] C. Weber, A. Läuchli, F. Mila, and T. Giamarchi, Phys. Rev. B **73**, 014519 (2006).  
[16] G. Kotliar, S. Savrasov, G. Pallson, and G. Biroli, Phys. Rev. Lett. **87**, 186401 (2001).  
[17] A. Georges, G. Kotliar, W. Krauth, and M. J. Rozenberg, Rev. Mod. Phys. **68**, 13 (1996).  
[18] C. Bolech, S. S. Kancharla, and G. Kotliar, Phys. Rev. B **67**, 075110 (2003); M. Capone *et al.*, Phys. Rev. B **69**, 195105 (2004).  
[19] B. Kyung, G. Kotliar, and A. M. S. Tremblay, Phys. Rev. B **73**, 205106 (2006).  
[20] B. Kyung *et al.*, Phys. Rev. B **73**, 165114 (2006).  
[21] M. Caffarel and W. Krauth, Phys. Rev. Lett. **72**, 1545 (1994).  
[22] The position of this peak scales as  $J = 4t^2/U$ .  
[23] The precise doping level versus the sodium content is still controversial among experimentalists. See M. Karppinen *et al.*, Chem. Mater. **16**, 1693 (2004); K. Takada *et al.*,

- J. Mater. Chem. **14**, 1448 (2004); L. Viciu, Q. Huang, [24] M. L. Foo *et al.*, Phys. Rev. Lett. **92**, 247001 (2004). and R. J. Cava, cond-mat/0603735.